Piggott, A. R. & Elsworth, D. (1996). *Géotechnique* 46, No. 4, 671–681

Displacement of formation fluids by hydraulic fracturing

A. R. PIGGOTT* and D. ELSWORTH†

Hydraulic fracturing of a geologic formation induces fluid flow within the formation in response to fracturing fluid loss and poroelasticity effects. Thus, hydraulic fracturing displaces the fluids that are distributed within the formation prior to fracturing, and may mobilize contaminants if applied in conjunction with groundwater contamination remediation. Fluid displacement is determined by coupling relations for hydraulic fracture extension to the temporal and spatial superposition of fundamental solutions for point fluid injection and a point dilation. Expressions are developed for three two-dimensional hydraulic fracture models for the limiting cases of high and low fracturing fluid loss to the formation. These results indicate that fluid displacement decreases with distance from the fracture and approaches an axisymmetric variation at greater than two fracture lengths from the well bore. Displacements induced by fluid loss and poroelasticity converge at greater than one fracture length from the fracture surface. Determination of fluid displacement for a hydraulic fracture treatment that may be typical in groundwater contamination remediation returns displacement magnitudes that are not likely to hamper the remediation effort.

KEYWORDS: contaminated land; groundwater; numerical modelling and analysis; pore pressures; seepage.

La fracturation hydraulique d'une formation géologique provoque l'écoulement des fluides dans la formation sous l'effet de la perte de fluides de fracturation et de la poroélasticité. Ainsi, la fracturation hydraulique déloge les fluides qui étaient répartis dans la formation avant la fracturation et, utilisée en conjonction avec la dépollution des eaux souterraines, peut mobiliser les contaminants. On établit le déplacement des fluides en mettant les rapports qui visent l'extension de la fracturation hydraulique en corrélation avec la superposition temporelle et spatiale des solutions fondamentales pour l'injection ponctuelle des fluides et une dilatation ponctuelle. Les auteurs formulent des expressions pour trois modèles bidimensionnels de fracture hydraulique pour les cas limites de forte et de faible perte de fluides de fracturation dans la formation. Les résultats obtenus indiquent que le déplacement des fluides diminue avec la distance par rapport à la fracture et se rapproche d'une variation axisymétrique à plus de deux longueurs de fracture du trou de sonde. Les déplacements provoqués par la perte de fluides et la poroélasticité convergent á plus d'une longueur de fracture de la surface de fracturation. La détermination du déplacement des fluides pour un traitement par fracturation hydraulique qui peut être représentatif dans la dépollution des eaux souterraines montre que ce déplacement est d'un ordre de grandeur qui est peu probable de faire obstacle aux efforts de dépollution.

INTRODUCTION

Hydraulic fracturing is frequently applied in the petroleum industry as a method of reservoir stimulation. In summary, hydraulic fracturing involves the injection of fluid into a formation section at a rate that is sufficient to initiate a fracture and then propagate the fracture outwards from the well bore. Proppant or acid is normally added to the fracturing fluid such that a conductive channel persists over the extent of the fracture following the closure of the fracture. During production, this conductive channel transmits the drawdown applied at the well bore over a larger area than would be affected without the fracture and results in an increased rate of hydrocarbon recovery, increasing the net present value of the resource.

Hydraulic fracturing has other potential applications in geomechanics, one of which is in groundwater contamination remediation. In pump-and-treat remediation schemes, hydraulic fracturing might be used to enhance contaminant recovery in

Manuscript received 12 June 1995; revised manuscript accepted 11 September 1995.
Discussion on this paper closes 3 March 1997; for further details see p. ii.

* National Water Research Institute, Burlington, Canada.
† Pennsylvania State University, University Park, USA.

a manner similar to that described for hydrocarbon production, i.e. to accelerate contaminant recovery and decrease the total cost of the operation. Hydraulic fracturing might also be used to form impermeable barriers to regulate contaminant migration and to install reactive curtains for the in situ degradation of contaminants. While still an emerging technology in groundwater contamination remediation, the application of hydraulic fracturing in this context has already been the subject of considerable research (Murdoch, Losonsky, Cluxton, Patterson, Klich & Braswell, 1991).

Mention of hydraulic fracturing in conjunction with groundwater remediation consistently elicits concern regarding the mobilization of the target contaminants by induced fluid flow within the formation. There are two mechanisms by which fluid flow is induced by hydraulic fracturing. The first mechanism is by fracturing fluid loss to the formation through the walls of the fracture; the second, and less intuitive, mechanism is by the poroelastic response of the formation to hydraulic fracturing. Extension of a hydraulic fracture within a formation results in the compression of the formation in proportion to the width of the fracture, and this in turn induces an excess fluid pressure by way of poroelasticity effects (Elsworth & Piggott, 1992). Both fracturing fluid loss and poroelasticity result in an advective fluid transport regime that leads to fluid migration away from the hydraulic fracture. If the contaminants that are distributed within the formation are mobile, then this induced motion may disperse the contamination over a larger area than was affected prior to fracturing. Thus, hydraulic fracturing may have a detrimental impact on the remediation effort if the increase in the dimension of the region of groundwater contamination is significant.

This paper describes the determination of the formation fluid displacement induced by several modes of fracture extension, adding to preliminary findings reported elsewhere (Piggott & Elsworth, 1994). Fluid displacement is defined as the distance that a reference fluid particle is displaced by the induced advective velocity regime. Hydrodynamic dispersion is not represented, as dispersion generates displacement magnitudes that are dependent on, and typically less than, the magnitudes induced by advective transport. For contaminants such as soluble metals, fluid displacement is a direct measure of contaminant mobilization, i.e. aqueous phase contaminants are likely to be mobilized in proportion to the motion of the formation fluid. For other forms of contaminants, such as non-aqueous phase liquids, fluid displacement indicates only the potential for contaminant mobilization, i.e. if fluid displacement is nominal, then it is likely that the motion of the contaminant is also limited.

HYDRAULIC FRACTURE EXTENSION

Figure 1 is a typical image of hydraulic fracture extension. Fracturing fluid injection through a perforated interval of a well generates fluid pressures that exceed the minimum in situ stress σ_{min} and the resistance of the formation to fracturing. This leads to the initiation of a fracture. Continued fluid injection causes the fracture to extend away from the well bore in the plane perpendicular to the direction of the minimum in situ stress, forming two symmetric fracture segments. In this illustration, the extension of the fracture in the vertical direction is restricted by an increase in the minimum in situ stress in the strata above and below the target horizon. Penetration of the fracture into these barriers is a function of fluid pressure, and therefore the height of the fracture varies along its length. In Fig. 1, the minimum in situ stress is horizontal and a vertical fracture is created. This is typical for rock at significant depth. Closer to the ground surface, the minimum in situ stress is often vertical and horizontal fractures are formed. Vertical fractures are likely in normally consolidated soils, while horizontal or subhorizontal fractures may form in overconsolidated soils. Fracture extension is regulated by the mechanical and hydraulic properties of the formation and the details of the fracture treatment. Thorough discussions of the mechanics of hydraulic fracture extension are presented in texts such as *Recent advances in hydraulic fracturing* (Society of Petroleum Engineers, Richardson) and *Reservoir stimulation* (Prentice Hall, Englewood Cliffs).

While sophisticated models of three-dimensional hydraulic fracture extension are available, the data

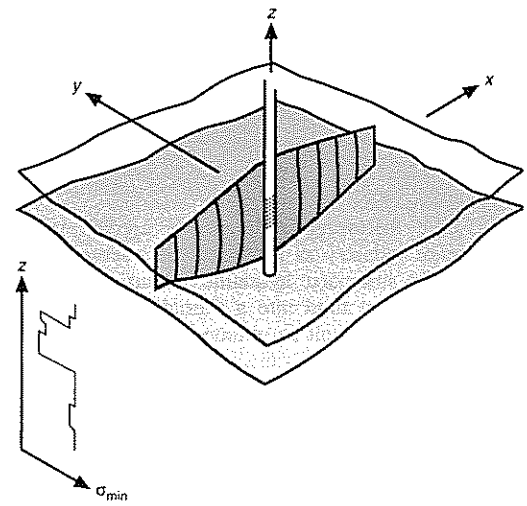

Fig. 1. Extension of a hydraulic feature

that are required as input to these models are infrequently known so simpler, two-dimensional models are more often applied in the analysis of hydraulic fracturing. Fig. 2 illustrates three two-dimensional hydraulic fracture models. The KGD (Khristianovic & Zheltov, 1955; Geertsma & de Klerk, 1969; Daneshy, 1973) and PKN (Perkins & Kern, 1961; Nordgren, 1972) models predict fracture extension in the direction of the x-axis with a constant height in the direction of the z-axis. Discussions of the validity of the KGD and PKN models are presented by Perkins (1973) and Geertsma & Haafkens (1979). The KGD model ignores the variation of fluid pressure in the direction of fracture extension and is valid for relatively short fractures (i.e. $L << H$). Furthermore, the model assumes constant width over the height of a fracture and requires shear displacement along the boundaries that define the height of the fracture. The PKN model assumes mechanical coupling over the height of the fracture with the variation of width in the direction of fracture extension expressed as a function of net pressure, which is defined as fracturing fluid pressure in excess of the minimum in situ stress. As a result, the PKN model is applicable to relatively long fractures (i.e. $L >> H$). The radial model (Perkins & Kern, 1961; Geertsma & de Klerk, 1969) predicts extension of the fracture in the plane of the x- and z-axis for vertical fractures and in the plane of the x- and y-axis for horizontal fractures. The radial model is applicable where the injection interval is small relative to the dimension of the fracture and where fracture extension is not significantly restricted by stress barriers, conditions typical for horizontal fractures.

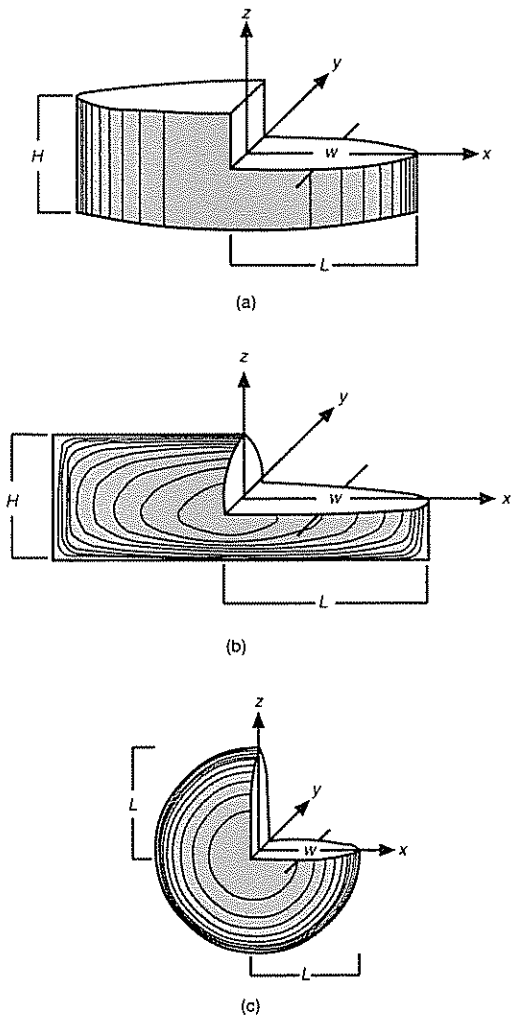

Fig. 2. Two-dimensional hydraulic fracture models (shading indicates variation of fracture width): (a) KGD; (b) PKN; (c) radial

Closed-form expressions for hydraulic fracture extension have been widely reported for the limiting cases of high and low fracturing fluid loss. The high fluid loss solutions apply when the rate of fluid loss to the surrounding formation approaches the pumping rate and fracture extension is regulated by fluid loss. The low fluid loss solutions apply when fluid loss is minimal and fracture extension is regulated by viscous flow and elasticity considerations. For a KGD fracture, the high and low fluid loss solutions are, respectively

$$L = \frac{Q}{2\pi C_L H} t^{1/2} \tag{1}$$

$$L = 0{\cdot}68\left(\frac{EQ^3}{16(1-\nu^2)\mu H^3}\right)^{1/6} t^{2/3} \tag{2}$$

where L is the length of the fracture at time t, E and ν are the Young's modulus and Poisson's ratio of the formation, Q and μ are the injection rate and viscosity of the fracturing fluid, C_L is the leak-off coefficient, and H is the height of the fracture. The extension of a PKN fracture subject to high fluid loss is also described by equation (1), while extension is described by

$$L = 0{\cdot}68\left(\frac{EQ^3}{16(1-\nu^2)\mu H^4}\right)^{1/5} t^{4/5} \tag{3}$$

for the case of low fluid loss. The high and low fluid loss solutions for a radial fracture are

$$L = \left(\frac{Q}{\pi^2 C_L}\right)^{1/2} t^{1/4} \tag{4}$$

$$L = 0{\cdot}74\left(\frac{EQ^3}{16(1+\nu)\mu}\right)^{1/9} t^{4/9} \tag{5}$$

Fracturing fluid loss

Fracturing fluid loss to the formation is the result of the difference between the fluid pressures inside the fracture and the surrounding formation. The rate of fluid loss through the two opposing surfaces of a fracture is generally approximated using

$$q = \frac{2C_L}{\sqrt{(t-\tau)}} \tag{6}$$

which is derived from the Carter relation for fracturing fluid loss (Carter, 1957). In equation (6), τ is the time at which the formation is first exposed to fracturing fluid. For the case of high fluid loss, the fracture closes at the end of pumping and the volume of fluid expelled into the formation is obtained by integration of equation (6) to yield

$$V = 4C_L\sqrt{t_p}\sqrt{\left(1-\frac{\tau}{t_p}\right)}\Delta A \tag{7}$$

where t_p is the duration of pumping and ΔA is an increment of the area of the fracture. Equation (7) assumes a particularly useful form when written specifically for each of the three fracture models. For the KGD and PKN models, equation (1) may be used to obtain

$$\frac{\tau}{t_p} = \left(\frac{x}{L_p}\right)^2 \tag{8}$$

$$C_L = \frac{Q}{2\pi HL_p}\sqrt{t_p} \tag{9}$$

where x is shown in Fig. 2 and L_p is the length of the fracture at the end of pumping. Substitution of these expressions into equation (7) results in

$$V = \frac{Qt_p}{2HL_p}\frac{4}{\pi}\sqrt{\left[1-\left(\frac{x}{L_p}\right)^2\right]}\Delta A \tag{10}$$

Similarly, equation (7) may be rewritten as

$$V = \frac{Qt_p}{\pi L_p^2}\frac{4}{\pi}\sqrt{\left[1-\left(\frac{r}{L_p}\right)^4\right]}\Delta A \tag{11}$$

for the radial model with $r^2 = x^2 + z^2$ for fracture extension in the plane of the x- and z-axis and $r^2 = x^2 + y^2$ for extension in the plane of the x- and y-axis.

Fracture width

The distribution of width within a hydraulic fracture is the result of the dislocation of the opposing fracture surfaces by the application of net fluid pressure to these surfaces. The KGD model assumes that fracture width is constant over the height of the fracture and varies along the length of the fracture in accordance with the elasticity solution of Sneddon & Elliott (1946). Thus, the variation of width within the fracture is given by

$$w = \langle w\rangle\frac{4}{\pi}\sqrt{\left[1-\left(\frac{x}{L}\right)^2\right]} \tag{12}$$

where $\langle w\rangle$ is the average width of the fracture. For the limiting case of low fluid loss, all the fracturing fluid is retained in the fracture and the average width of the fracture at the end of pumping may be determined from the volume and area of the fracture Qt_p and $2HL_p$. As a result, the volume of the formation medium that is displaced by the inflation of the fracture is given by

$$V = \frac{Qt_p}{2HL_p}\frac{4}{\pi}\sqrt{\left[1-\left(\frac{x}{L_p}\right)^2\right]}\Delta A \tag{13}$$

The PKN model uses the elasticity solution of Sneddon & Elliott (1946) to describe the variation of width over the height of the fracture. Combination of this with the variation of net pressure along the length of a PKN fracture given by Nolte (1990) allows the distribution of width over the length and height of a PKN fracture to be expressed as

$$w = \langle w\rangle\frac{16}{3\pi}\left(1-\frac{|x|}{L}\right)^{1/3}\sqrt{\left[1-\left(\frac{2z}{H}\right)^2\right]} \tag{14}$$

which translates to

$$V = \frac{Qt_p}{2HL_p}\frac{16}{3\pi}\left(1-\frac{|x|}{L_p}\right)^{1/3}\sqrt{\left[1-\left(\frac{2z}{H}\right)^2\right]}\Delta A \tag{15}$$

The radial model predicts the variation of fracture width using the elasticity solution of Sneddon (1946), and the resulting relation for the width distribution is

$$w = \langle w\rangle\frac{3}{2}\sqrt{\left[1-\left(\frac{r}{L}\right)^2\right]} \tag{16}$$

Again, the average width of the fracture may be determined from the volume and area of the fracture Qt_p and πL_p^2 and the dilation of the formation due to the inflation of the fracture is given by

$$V = \frac{Qt_p}{\pi L_p^2}\frac{3}{2}\sqrt{1-\left(\frac{r}{L_p}\right)^2}\Delta A \tag{17}$$

FLUID DISPLACEMENT DUE TO POINT INJECTION AND DILATION

The influences of fracturing fluid loss and poroelasticity effects on formation fluid displacement are determined through the fundamental solutions for point fluid injection and a point dilation. The solution for point fluid injection models fracturing fluid loss to the formation, while the solution for a point dilation models the poroelasticity effects resulting from the evolution of fracture width. Fig. 3 illustrates fluid displacement due to point fluid injection or a point dilation. Either of these processes centred at $\underline{x}^{\mathrm{T}} = [x, y, z]$ result in a fluid displacement magnitude of Δ_{R} at an observation location $\underline{x}_0$, where the distance between the source and observation points is

$$R = \sqrt{[(x_0 - x)^2 + (y_0 - y)^2 + (z_0 - z)^2]} \tag{18}$$

and the orientation of the displacement magnitude relative to the co-ordinate axes is given by

$$\underline{u} = \frac{1}{R}[x_0 - x, y_0 - y, z_0 - z] \tag{19}$$

Fluid displacement due to point fluid injection

The hydraulic head induced by continuous point fluid injection in an infinite, homogeneous, isotropic, three-dimensional domain is (Carslaw & Jaeger, 1986)

$$h = \frac{Q}{4\pi KR}\operatorname{erfc}(\xi) \tag{20}$$

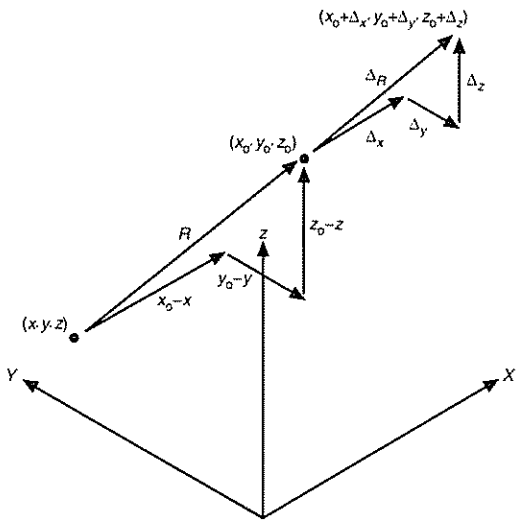

Fig. 3. Geometry of fluid displacement due to point fluid injection or point dilation

where K is the hydraulic conductivity of the formation, and erfc (ξ) denotes the complementary error function of dimensionless time

$$\xi = \frac{R}{\sqrt{(4Dt)}} \tag{21}$$

with D defined as the hydraulic diffusivity of the formation. The resulting advective velocity, measured in the radial direction, is obtained by differentiating equation (20) with respect to R and conditioning the result using the porosity of the formation n (Freeze & Cherry, 1979) to yield

$$v_{\mathrm{R}} = \frac{Q}{4\pi nR^2}\left(\operatorname{erfc}(\xi) + \frac{2}{\sqrt{\pi}}\xi\,\mathrm{e}^{-\xi^2}\right) \tag{22}$$

Integration of equation (22) with respect to time returns the fluid displacement at the observation location

$$\Delta_{\mathrm{R}} = \frac{Qt}{4\pi nR^2} \times\left(-2\xi^2 + \frac{2}{\sqrt{\pi}}\xi\,\mathrm{e}^{-\xi^2} + 2\xi^2\operatorname{erf}(\xi) + \operatorname{erfc}(\xi)\right) \tag{23}$$

where erf (ξ) denotes the error function of dimensionless time.

Equation (23) states the fluid displacement induced by continuous, constant rate injection. The principle of superposition allows this result to be used to determine the displacement corresponding to constant rate injection with a finite duration (Earlougher, 1977). A second application of superposition then allows this result to be used to determine the displacement due to temporally varying injection. Following this approach, fluid displacement is given by

$$\Delta_{\mathrm{R}} = \frac{V}{4\pi nR^2} \tag{24}$$

in the limit as $t \to \infty$ where V denotes the total volume of fluid injected into the formation. Displacement in the directions of the co-ordinate axes is given by

$$\underline{\delta} = \frac{V}{4\pi nR^2}\underline{u} \tag{25}$$

where, for the case of hydraulic fracture extension, V is determined using equation (10) or (11).

Fluid displacement due to a point dilation

The hydraulic head induced by a point dilation (i.e. an instantaneous volume change) in an infinite, homogeneous, isotropic three-dimensional domain is (Elsworth & Voight, 1992)

$$h = \frac{D\Delta V}{\pi K R^3} \frac{\xi^3}{\sqrt{\pi}} e^{-\xi^2} \tag{26}$$

where ξ is dimensionless time as defined in equation (21) and ΔV is the magnitude of the point dilation. Equation (26) yields an advective velocity of

$$v_R = \frac{2D\Delta V}{\pi n R^4} \frac{\xi^5}{\sqrt{\pi}} e^{-\xi^2} \tag{27}$$

in the radial direction. The fluid displacement resulting from the point dilation is determined by integrating equation (27) with respect to time, and assumes the form

$$\Delta_R = \frac{\Delta V}{4\pi n R^2} \tag{28}$$

in the limit as $t \to \infty$.

Application of superposition allows the fluid displacement due to temporally varying dilation to be calculated from the solution for a single event. This result has the same form as equation (24), where V denotes the summation of the dilation increments ΔV. The resulting displacement contribution may also be partitioned into components in the directions of the co-ordinate axes and, logically, the result has the same form as equation (25), where V is given by equation (13), (15) or (17).

FLUID DISPLACEMENT DUE TO HYDRAULIC FRACTURE EXTENSION

The variation of fluid loss and dilation over the extent of a hydraulic fracture is represented by the spatial superposition of displacement increments computed using equation (25). In integral form, this translates to

$$\underline{\Delta} = \int_A \underline{\delta}\, dA \tag{29}$$

where A is the area of the fracture and dA indicates an infinitesimal increment of this area. This approach is based on the assumption that the velocity applied to the reference fluid particle is unchanged with respect to the motion of the particle, i.e. the particle experiences a velocity history that is equal to that applied at the initial position of the particle. This assumption is accurate provided that the displacement of the particle is small relative to the spatial variation of fluid displacement, and is appropriate for resonable values of the formation and fracture treatment parameters (Piggott, 1995).

The fluid displacement induced by a hydraulic fracture subject to high fracturing fluid loss to the formation is due solely to fluid loss as fracture volume, and therefore poroelasticity effects, are negligible. For a KGD or PKN fracture, displacement is determined using equation (25), where the volume of fluid injected into the formation per unit area is given by equation (10). Substitution of these relations into equation (29), with $dA = dx\, dz$, yields

$$\underline{\Delta} = \frac{Qt_p}{2HL_p n} \int_{-H/2}^{H/2} \int_{-L_p}^{L_p} \frac{1}{\pi^2} \sqrt{\left[1 - \left(\frac{x}{L_p}\right)^2\right]} \times \frac{1}{R^2} \underline{u}\, dx\, dz \tag{30}$$

Transformation of the geometry of the scenario into the dimensionless form

$$\underline{x}_d = \frac{1}{L_p} \underline{x} \tag{31}$$

allows equation (30) to be rewritten as

$$\underline{\Delta} = \frac{Qt_p}{2HL_p n} \int_{-H_d/2}^{H_d/2} \int_{-1}^{1} \frac{1}{\pi^2} \sqrt{(1 - x_d^2)} \frac{1}{R_d^2} \underline{u}_d\, dx_d\, dz_d \tag{32}$$

The fluid displacement distribution for a radial fracture subject to high fluid loss is determined by substituting equation (11) into equation (25) and substituting the result into equation (29), with $dA = r\, dr\, d\theta$. This leads to

$$\underline{\Delta} = \frac{Qt_p}{\pi L_p^2 n} \int_0^{2\pi} \int_0^1 \frac{1}{\pi^2} r_d \sqrt{(1 - r_d^4)} \frac{1}{R_d^2} \underline{u}_d\, dr_d\, d\theta \tag{33}$$

where the co-ordinates of the source point are given by

$$\underline{x}_d^T = (r_d \cos\theta,\ 0,\ r_d \sin\theta) \tag{34}$$

For the case of low fracturing fluid loss, fluid displacement is due solely to the poroelastic response of the formation. For a KGD fracture, substitution of equation (13) into equation (25) and substitution of the result into equation (29) yields

$$\underline{\Delta} = \frac{Qt_p}{2HL_p n} \int_{-H_d/2}^{H_d/2} \int_{-1}^{1} \frac{1}{\pi^2} \sqrt{(1 - x_d^2)} \frac{1}{R_d^2} \underline{u}_d\, dx_d\, dz_d \tag{35}$$

The analogous result is

$$\underline{\Delta} = \frac{Qt_p}{2HL_p n} \int_{-H_d/2}^{H_d/2} \int_{-1}^{1} \frac{4}{3\pi^2} (1 - |x_d|)^{1/3} \times \sqrt{\left[1 - \left(\frac{2z_d}{H_d}\right)^2\right]} \frac{1}{R_d^2} \underline{u}_d\, dx_d\, dz_d \tag{36}$$

for a PKN fracture and is obtained using equation (15) in place of equation (13). Finally, the fluid displacement due to poroelasticity effects is given by

$$\underline{\Delta} = \frac{Qt_p}{\pi L_p^2 n} \int_0^{2\pi} \int_0^1 \frac{3}{8\pi} r_d \sqrt{(1 - r_d^2)} \frac{1}{R_d^2} \underline{u}_d \, dr_d \, d\theta \tag{37}$$

for a radial fracture, where equation (17) represents the distribution of fracture width.

The integral quantities in equations (32), (33) and (35)–(37) are dimensionless. The dimensional values of displacement are contributed by the parameter group that pre-multiplies each of the integral quantities. Thus, fluid displacement may be expressed as

$$\underline{\Delta} = \frac{Qt_p}{2HL_p n} \underline{\Delta}_d \tag{38}$$

for KGD and PKN fractures and as

$$\underline{\Delta} = \frac{Qt_p}{\pi L_p^2 n} \underline{\Delta}_d \tag{39}$$

for radial fractures. Logically, the potential for contaminant mobilization is related to the total displacement magnitude, whose dimensionless component is given by

$$\Delta_{d,T} = \sqrt{\underline{\Delta}_d \cdot \underline{\Delta}_d} \tag{40}$$

Representation of fluid displacement distributions in dimensionless form is a convenient method of depicting the distributions. However, displacement distributions that are similar when expressed in dimensionless form may not be similar when expressed in dimensional form, due to differences in the fracture geometry, fracturing fluid volume, and formation porosity indicated in equations (38) and (39).

Representation of hydraulic boundaries

Hydraulic boundaries in the vicinity of a fracture have a pronounced impact on fluid displacement. In this analysis, hydraulic boundaries are idealized as impermeable or constant head features of infinite, planar geometry. The influence of a hydraulic boundary on fluid displacement is determined through the application of image theory (Earlougher, 1977; Kruseman & de Ridder, 1983), reflecting the source across the boundary and assigning fluid injection or dilation to the image. For the case of an impermeable boundary, the image has the same sense as the source (e.g. fluid injection is assigned to the source and image). For the case of a constant head boundary, the image has the opposite sense (e.g. fluid injection is assigned to the source, fluid withdrawal to the image). The location of an image is determined from the geometry of the source and boundary using methods of linear algebra (Anton, 1981). In cases of more than one boundary, second generation images are required to correct for spurious contributions imparted by the first generation images, and third generation images are required to correct for the second generation images. In practice, the formation of images is terminated when the addition of a generation of images results in only a nominal change in the computed fluid displacement. The influence of a source and its images is incorporated into equations (32), (33) and (35)–(37) through the substitution

$$\frac{1}{R_d^2} \underline{u}_d = \sum_i \pm \frac{1}{R_{d,i}^2} \underline{u}_{d,i} \tag{41}$$

where $R_{d,i}$ and $\underline{u}_{d,i}$ are computed using the source and image locations, and the sense of the increments is defined by the nature of the boundaries that form the images.

Dimensionless fluid displacement distributions

The integrand functions in the relations for fluid displacement are distinctly peaked in the vicinity of the fracture and are relatively uniform further from the fracture. In addition, the evaluation of these functions involves considerable computational effort. These characteristics justify the use of an adaptive integration scheme (Press, Teukolsky, Vetterling & Flannery, 1992). In the following, integration is performed using Gauss–Legendre quadrature (Atkinson, 1978), where the number of quadrature points representing the two ranges of integration is increased until a convergent estimate of the integral is obtained.

Figure 4 shows the distributions of fluid displacement computed for the cases of high fracturing fluid loss to the formation (i.e. displacement due entirely to fluid loss) and low fracturing fluid loss to the formation (i.e. displacement due entirely to poroelasticity) for the KGD, PKN, and radial hydraulic fracture models. The barriers that restrict the height of KGD and PKN fractures are typically impermeable and the results shown for the KGD and PKN fractures apply to an arbitrary fracture height of $H_d = 1$ with horizontal, impermeable boundaries located at $z_{d,o} = \pm 0{\cdot}5$. Displacement is presented as a function of $x_{d,o}$ and $y_{d,o}$ with $z_{d,o} = 0$ for all three models. For the KGD and PKN models, displacement is also shown as a function of $y_{d,o}$ and $z_{d,o}$ with $x_{d,o} = 0$. Displacement is symmetric about the y-axis for the radial model, and therefore the indicated results fully characterize these distributions.

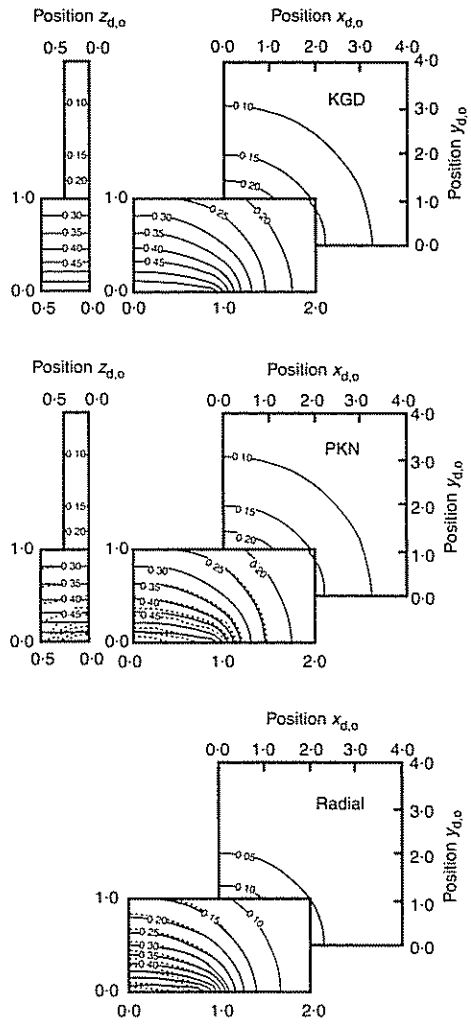

Fig. 4. Dimensionless fluid displacements induced by fracturing fluid loss (solid lines) and poroelasticity effects (broken lines): insets show details of corresponding displacement distributions in the vicinity of the fractures

In the vicinity of the fracture, the contours of displacement parallel the fracture surface and the direction of fluid displacement is away from the fracture surface. Displacement decreases rapidly with distance from the fracture surface. Fluid displacements due to fluid loss and poroelasticity are equal for the KGD model as a result of the similarity of equations (10) and (13). For the PKN and radial models, fluid displacements due to fluid loss and poroelasticity differ in the vicinity of the fracture but converge with increasing distance from the fracture. For the PKN model, the displacement induced by poroelasticity is a function of $z_{d,o}$ in the vicinity of the fracture, reaching a peak at $z_{d,o} = 0$, but is independent of $z_{d,o}$ further from the fracture. This is the result of the variation of fracture width over the height of a PKN fracture, as indicated in equation (15).

It is not coincidental that the displacement distributions corresponding to fluid loss and poroelasticity are very nearly equal beyond the immediate vicinity of the fracture. Both distributions reflect the total volume of fluid injected into the formation where this influence is partitioned according to equation (10) or (11) in the case of fluid loss and equation (13), (15) or (17) in the case of poroelasticity. Increasing the distance between the fracture and observation location emphasizes the influence of the positioning of the observation location relative to the influence of the partitioning of fluid loss or dilation. Under these conditions, the geometry of the configuration is dominant over the details of fracture extension in defining the displacement distribution.

The distributions of fluid displacement in Fig. 4 display an axisymmetric variation about the well bore at some distance from the well bore. This suggests that the influence of distributing fluid loss and dilation over the extent of the fracture diminishes with distance from the well bore. The displacement induced by fluid injection at the well bore, rather than over the area of the fracture, may be obtained from the solution for point injection reported in Piggott & Elsworth (1994) for the case of KGD and PKN fractures that are constrained by permeability barriers coincident with the top and bottom of the fracture. In terms of dimensionless displacement, the resulting displacement distribution is given by

$$\Delta_{d,R} = \frac{1}{\pi}\frac{1}{R_d} \tag{42}$$

The analogous result for a radial fracture that is not constrained by permeability barriers is

$$\Delta_{d,R} = \frac{1}{4}\frac{1}{R_d^2} \tag{43}$$

Figure 5 compares the fluid displacement magnitudes along the x- and y-axis computed for distributed fluid loss and dilation to the axisymmetric approximations in equations (42) and (43). The displacement magnitudes along these axes bracket the range of values for any equivalent distance from the well bore R_d. Points along the x-axis are closest to the fracture for any given value of R_d and exhibit the maximum magnitudes for that value of R_d, and points along the y-axis are furthest from the fracture for any given value of R_d and exhibit the minimum magnitudes for that value of R_d. The displacements predicted by the

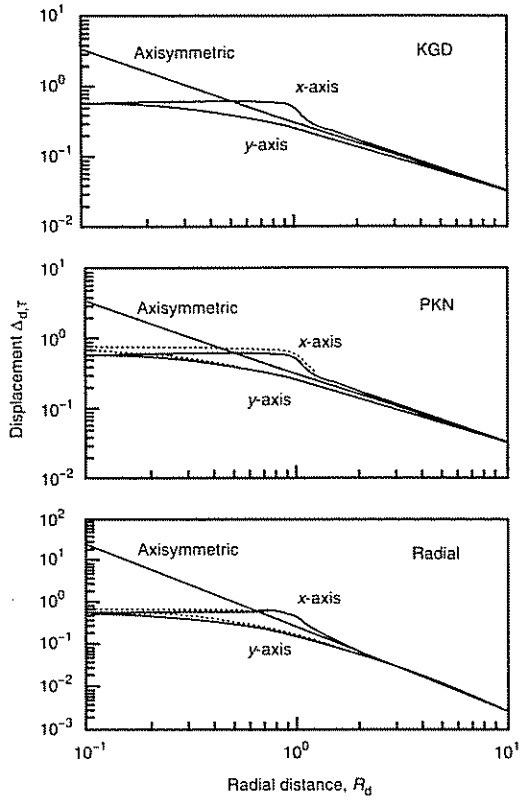

Fig. 5. Comparison of fluid displacement due to distributed fluid loss and dilation (*x*- and *y*-axis with the displacement predicted for fluid injection at the well bore (axisymmetric)

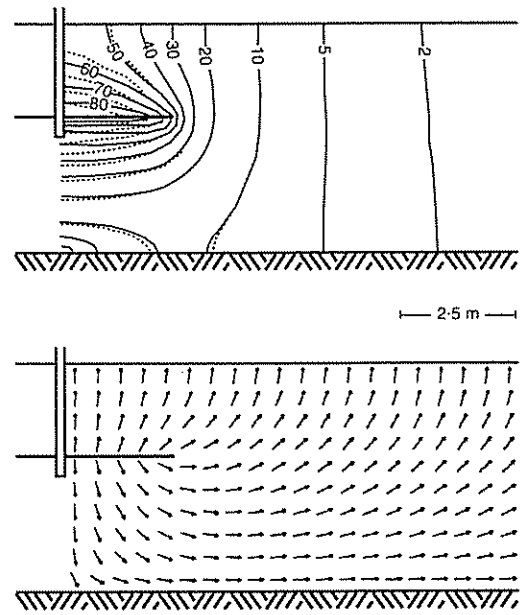

Fig. 6. Fluid displacement for a hydraulic fracture treatment performed in a groundwater contamination remediation context: (top) variation of fluid displacement (mm); (bottom) orientation of the displacement of the fluid magnitude

axisymmetric approximations are nearly equal to the results for distributed fluid loss and dilation at greater than two fracture lengths from the well bore, but greatly overestimate the distributed results closer to the well bore. Thus, fluid displacement can be accurately predicted using equations (42) and (43) at greater than two fracture lengths from the well bore. Closer to the well bore, displacement must be determined using the solutions for distributed fluid loss or dilation.

FLUID DISPLACEMENT DUE TO A TYPICAL HYDRAULIC FRACTURE TREATMENT

Figure 6 shows the distribution of fluid displacement for what may be typical of hydraulic fracturing performed in the context of groundwater contamination remediation; the corresponding formation and fracture treatment parameters are within the range of values reported by Murdoch (1995). Here, the resulting fracture is horizontal and radial with a length of 2·5 m and occurs at a depth of 2 m, the porosity of the formation is 0·3, the thickness of the formation is 5 m, and the total volume of fluid injected into the fracture is 0·75 m^3. The lower boundary represents contact with an impermeable formation, while a constant head is assumed at the upper boundary to represent the location of the water table.

The displacement distribution is symmetric about the well bore, and Fig. 6 shows the variation of displacement for any section through the well bore. Displacement magnitudes are relatively small, with a peak value of approximately 100 mm in the vicinity of the fracture, and decrease rapidly with increasing distance from the fracture. Fluid displacement above the fracture is greater than that below the fracture as the result of elevated flow toward the water-table. The impact of the hydraulic boundaries on the pattern of fluid displacement is also apparent in the orientation of the displacement magnitudes. The magnitudes of the displacements induced by fluid loss and poroelasticity deviate in the immediate vicinity of the fracture but are indistinguishable at greater than one fracture length from the fracture. The orientations of the displacements induced by fluid loss and poroelasticity are indistinguishable throughout the section.

There is little reason to suspect that the displacement magnitudes shown in Fig. 6 would

hamper a remediation effort. The peak displacement magnitude of 100 mm is a small fraction of the 2·5 m length of the fracture and, since the distribution of contamination is logically of comparable size, displacement is equally small with respect to the extent of contamination. While not definitive, this example does suggest that the fluid displacement induced by hydraulic fracturing may not be a deterrent to the application of hydraulic fracturing in conjunction with groundwater contamination remediation.

CONCLUSIONS

Hydraulic fracturing of a geologic formation displaces the fluid that is distributed within the formation prior to fracturing through fracturing fluid loss and poroelasticity effects. When hydraulic fracturing is applied in the context of groundwater contamination remediation, the accompanying fluid displacement may mobilize the target contaminants and hamper the remediation effort.

The relations developed in this paper predict the fluid displacement accompanying the extension of KGD and PKN, radial hydraulic fractures for the limiting cases of high and low fracturing fluid loss. These limiting cases correspond to flow that is induced entirely by fluid loss and poroelasticity effects, respectively. Both the fluid displacement mechanism and the geometry of the created fracture must be known to predict fluid displacement in the immediate vicinity of a fracture. Displacements for the cases of high and low fluid loss are very nearly equal at greater than one fracture length from the fracture surface and therefore only fracture geometry must be known to predict fluid displacement in this region. Fluid displacement at greater than two fracture lengths from the well bore may be predicted by injection at the well bore, thus neither the mechanism of fluid displacement nor the geometry of the created fracture need be known.

The fluid displacements computed for a hydraulic fracture treatment that may be typical in groundwater contamination remediation are small and are not likely to hamper the remediation effort. The expressions for fluid displacements due to hydraulic fracturing presented in this paper may be used to test this conclusion for other sets of formation and fracture treatment parameters.

Expressions for fluid displacement were developed for the cases of high and low fluid loss in response to the existence of matching closed-form relations for fracture extension. Similar expressions are not easily obtained for the case of intermediate fluid loss where both fluid loss and poroelasticity contribute to fluid displacement. In this case, fracture extension must be determined by numerical simulation and the relations for fluid displacement must be revised to incorporate the numerical results. It is, however, possible to approximate the case of intermediate fluid loss using fracture efficiency η, defined as the ratio of the volume of fluid retained in a fracture to the total volume of fluid injected into the fracture. An efficiency of $\eta = 0$ indicates high fluid loss while a value of $\eta = 1$ indicates low fluid loss. It follows that the fluid displacement induced by a fracture of known efficiency can be approximated as

$$\Delta_T = (1 - \eta)\Delta_{T,\text{high}} + \eta\Delta_{T,\text{low}} \tag{44}$$

where $\Delta_{T,\text{high}}$ and $\Delta_{T,\text{low}}$ are the displacements computed for high and low fluid loss. This approximation circumvents the determination of fracture extension but still requires knowledge of the model that best represents fracture extension and of the geometry of the created fracture. Thus, this approximation is most useful in cases where fracture geometry is known from in situ observations.

ACKNOWLEDGEMENTS

The authors thank Hugo Morales of Dowell Schlumberger Incorporated for his assistance in compiling the closed-form solutions for fracture extension.

REFERENCES

Anton, H. (1981) *Elementary linear algebra*. New York: Wiley.

Atkinson, K. E. (1978). *An introduction to numerical analysis*. New York: Wiley.

Carslaw, H. S. & Jaeger, J. C. (1986). *Conduction of heat in solids*. Oxford: Oxford University Press.

Carter, R. D. (1957). Appendix to 'Optimum fluid characteristics for fracture extension' by G. C. Howard and C. R. Fast. *Drill. Prod. Pract.* **267**.

Daneshy, A. A. (1973). On the design of vertical hydraulic fractures. *J. Pet. Technol.* **25**, 83–93.

Earlougher, R. C. (1977). *Advances in well test analysis*. New York: Society of Petroleum Engineers.

Elsworth, D. & Piggott, A. R. (1992). Hydrofracturing characterization through the monitoring of induced pore fluid pressures. *Proceedings of international conference on flow through porous media: fundamentals and reservoir engineering applications*. Moscow: Institute for Problems in Mechanics, Russian Academy of Sciences.

Elsworth, D. & Voight, B. (1992). Theory of dike intrusion in a saturated porous solid. *J. Geophys. Res.* **97B**, 9105–9117.

Freeze, R. A. & Cherry, J. A. (1979). *Groundwater*. Englewood Cliffs: Prentice Hall.

Geertsma, J. & de Klerk, F. (1969). A rapid method of predicting width and extent of hydraulically induced fractures. *J. Pet. Technol.* **21**, 1571–1581.

Geertsma, J. & Haafkens, R. (1979). A comparison of the theories for predicting width and extent of vertical hydraulically induced fractures. *J. Energy Res. Technol.* **101**, 8–19.

Khristianovic, S. A. & Zheltov, Y. P. (1955). Formation of vertical fractures by means of highly viscous liquid. *Proc. 4th World Petroleum Conf.*, Section II, 579–586.

Kruseman, G. P. & de Ridder, N. A. (1983). *Analysis and evaluation of pumping test data*. Wageningen: International Institute for Land Reclamation and Improvement/ILRI.

Murdoch, L. C. (1995). Forms of hydraulic fractures created during a field test in overconsolidated glacial drift. *Q. J. Engng Geol.* **28**, 23–35.

Murdoch, L. C., Losonsky, G., Cluxton, P., Patterson, B., Klich, I. & Braswell, B. (1991). *Feasibility of hydraulic fracturing to improve remedial actions*. USEPA/600/S2-91/012, Washington, DC: US Environmental Protection Agency.

Nolte, K. G. (1990). Fracturing pressure analysis: deviations from ideal assumptions. *Proc. 65th Ann. Technical Conf. and Exhibition of the Society of Petroleum Engineers*, 839–854. Richardson: Society of Petroleum Engineers.

Nordgren, R. P. (1972). Propagation of a vertical hydraulic fracture. *Soc. Pet. Engrs J.* **253**, 306–314.

Perkins, T. K. (1973). Discussion of 'On the design of vertical hydraulic fractures' by A. A. Daneshy. *J. Pet. Technol.* **25**, 93–97.

Perkins, T. K. & Kern, L. R. (1961). Widths of hydraulic fractures. *J. Pet. Technol.* **13**, 937–949.

Piggott, A. R. (1995). *Static and dynamic calculation of formation fluid displacement induced by hydraulic fracturing*. National Water Research Institute, Contribution 95-25.

Piggott, A. R. & Elsworth, D. (1994). Formation fluid displacement induced by hydraulic fracturing. *Proc. 8th Int. Conf. on Computer Methods and Advances in Geomechanics*, 1627–1632.

Press, W. H., Teukolsky, S. A., Vetterling, W. T. & Flannery, B. P. (1992). *Numerical Recipes in FORTRAN: the Art of Scientific Computing*, 2nd edn. Cambridge: Cambridge University Press.

Sneddon, I. N. (1946). The distribution of stress in the neighbourhood of a crack in an elastic solid. *Proc. R. Soc. Lond.* **187A**, 229–260.

Sneddon, I. N. & Elliott, H. A. (1946). The opening of a Griffith crack under internal pressure. *Q. Appl. Math.* **4**, 262–267.